18th International Conference on Structural Mechanics in Reactor Technology (SMiRT 18)
Beijing, China, August 7-12, 2005
SMiRT18-J07-3

EVALUATION OF FRETTING WEAR DATA WITH THE AID OF MECHANISM-MAPS

Jakob Knudsen*
Malmö University
SE-20506 Malmö, Sweden
Phone: +46-40-6657690
Fax: +46-40-6657135
E-mail: tsjakn@ts.mah.se

Ali R. Massih
Malmö University

ABSTRACT

The concept of the fretting map, which identifies four separate regimes of fretting wear, namely, stick, mixed stick-slip, gross slip and reciprocating sliding, is re-assessed with respect to its experimental database. It is shown that the scatter in data is too large to draw definite conclusions regarding the boundaries of the various fretting regimes. Furthermore, the database is extended with some results relevant to fretting wear of nuclear reactor components. An alternative approach, using dimensionless parameters, namely the wear rate, the contact pressure, the sliding amplitude and the coefficient of wear, is proposed for constructing fretting maps. The proposed map is explored in reference to certain transition criteria for determining the boundaries between the different regimes of fretting.

Keywords: Fretting wear; Fretting map; Wear susceptibility; Critical slip range.

1 INTRODUCTION

Fretting wear is a concern for many components in nuclear power plants, e.g. steam generator tubes and fuel rods (Pettigrew, Taylor, Fisher, Yetsir and Smith 1998). Steam generator tubes are designed with small clearances between the tubes and their support to accommodate thermal expansion. Fuel rods, on the other hand, are initially fixed by support springs, but a gap between springs and rods might develop during operation due to irradiation induced creep down of fuel cladding, spring relaxation, etc. The common denominator between both components is that they are both subject to flow-induced vibration by the surrounding fluid (Au-Yang 2001). The vibration causes impact and sliding against the supporting structure. Consequently wear of these components must be taken into account. In nuclear reactor components, the rate of wear is usually quantified in terms of a quantity called the work rate, which is the average energy dissipated at the contact, see e.g. (Fisher, Chow and Weckwerth 1994, Fisher, Chow and Weckwerth 1995). The energy dissipation during a fretting cycle depends on the fretting regime, namely, stick, mixed stick-slip, gross slip and reciprocating sliding regimes. Thus to predict the lifetime of such components it is necessary determine the fretting wear rate, which in turn depends on the prevailing modes of fretting.

Fretting refers to a small oscillatory motion between two solid surfaces in contact, with amplitudes roughly in the range 10 to 100 μm. The direction of motion can be tangential and/or normal to the surfaces. Experience shows that this type of motion causes surface degradation, which is usually called fretting damage or fretting wear (Hutchings 1992). Fretting damage is an outcome of a number of effects, which include the state of mechanical contact (geometry, direction and magnitude of forces, displacement amplitudes and frequency of oscillation) and the environmental effects such as temperature and medium (water, air, etc.) and materials comprising the fretting pair. Hence the number of parameters participating in fretting process can be quite large.

One approach to systematisation of fretting data is to construct wear mechanism maps fashioned after Lim and Ashby (1987), who evaluated the data on the volume lost from the surface, due to contact-sliding from various sources, with specimens of different shapes and sizes, by correlating some dimensionless parameters, a *parameter*

*Corresponding author

space, which best describe the process of wear. The purpose of the map is to show how the different damage effects interface and also to identify the dominant effect for any given set of conditions. Vingsbo and Söderberg (1988) introduced the concept of fretting map to distinguish and identify the different regimes of fretting from dynamic measurements of tangential force and displacements. In particular, the Vingsbo-Söderberg map is a diagram displaying the various regimes, in which different modes of fretting dominate. A curve is depicted in terms of two pertinent variables (e.g. the wear rate vs. displacement) with boundaries representing threshold values for the transition from one regime to another. Subsequently, other fretting maps have been proposed, relating the threshold amplitude at the onset of gross slip to the applied normal load, frequency of vibration and material hardness (Odfalk and Vingsbo 1990, Vingsbo, Odfalk and Shen 1990). These authors showed that the threshold amplitude increases with increasing normal load and frequency and decreases with increasing hardness. The threshold values were identified from recordings of the variation of tangential forces and displacements with time. Vingsbo and Söderberg, based on their own experimental results and literature data, constructed the fretting maps, which although stated to be schematic, they include quantitative threshold values for various regimes of fretting (Vingsbo and Söderberg 1988). Vingsbo and Söderberg, however, did not juxtapose the experimental data on the diagrams in order to show the reliability of the threshold values. We should point out that the threshold lines in the Vingsbo-Söderberg map are purely empirical with no quantitative theoretical justification. Vincent, Berthier and Godet (1992) developed this technique further and introduced the concept of running condition fretting map (RCFM) which maps the characteristics of the fretting regimes during the experiment. The RCFM is generated from analysis of a 3-dimensional plot of the sliding amplitude D, tangential load T and time. These authors identified three types of $T-D$ cycles in a fretting system, namely, a closed cycle indicating stick conditions, an elliptic cycle resulting from mixed stick-slip conditions and a trapezoidal cycle characterising the gross slip regime. The general shapes of these $T-D$ cycles are believed to be universal for a fretting system and not limited to metal/metal systems, e.g., they are applicable to metal/polymer contacts (Dahmani, Vincent, Vannes, Berthier and Godet 1992) and metal/reinforced polymer contacts (Turki, Salvia and Vincent 1993). These 3-d plots are also used to study and distinguish the mechanism for the transfer of velocity over the contact interface (Dahmani et al. 1992).

The transition between the fretting regimes is determined experimentally by studying the change in the shape of the aforementioned $T-D$ cycles. Fouvry, Kapsa and Vincent (1995) proposed several criteria based on Mindlin's theory to determine the transition between mixed stick-slip and gross slip fretting regimes. The criteria were formulated with an energy ratio and a displacement ratio. At the transition boundary, these ratios have specific constant values, which can be determined experimentally once the tangential compliance of the experimental rig is known (Fouvry et al. 1995). Considering the evolution of fretting, the two regions, mixed stick-slip and gross slip, provide a map with three domains, mixed stick-slip, mixed slip and gross slip. The second domain comprises experimental conditions which evolve from mixed stick-slip to gross slip or vice versa during the test (Fouvry, Kapsa and Vincent 1996). Cracks form at the edge of the contact region during mixed stick-slip, either due to excessive plastic strains (Johnson 1995) or fatigue (Fouvry, Kapsa, Vincent and Dang Van 1996, Szolwinski and Farris 1996). During gross slip, wear is the dominant damage process. In this regime a linear relationship between wear volume and the accumulated dissipated energy has been found (Fouvry, Kapsa and Vincent 1996).

The aim of this note is to first juxtapose the aforementioned experimental data on the wear rate versus displacement map to see how well the data compare with the Vingsbo-Söderberg threshold lines. Moreover, using the available experimental data, we attempt to present alternative diagrams, which may distinguish the different regimes of fretting more adequately. Our analysis is based on the elastic theory of oscillating bodies in contact (Mindlin 1949, Mindlin, Mason, Osmer and Deresiewicz 1951, Mindlin and Deresiewicz 1953). Section 2 outlines the concept fretting map. Method of analysis is presented in section 3. In section 4 we attempt to systematise the available fretting data. Fretting data are discussed in the light of suggested fretting maps in section 5. We close the paper by some concluding remarks in section 6.

2 FRETTING MAP

Vingsbo and Söderberg, from their experiments, by comparing the measured dynamic force curves (force vs. displacement) with the observed topographical characteristics of the associated wear scars, could identify three different regimes of fretting contact (Vingsbo and Söderberg 1988). Based on these investigations, they proposed a map dividing the parameter space into regions where different fretting wear mechanisms are acting. The fretting contact regimes are classified by different stick slip conditions as follows:

1. *Stick regime => Low damage fretting.* Limited surface damage occurs due to oxidation and wear. No fatigue crack formation (up to 10^6 cycles) is observed.

2. *Mixed stick-slip regime => Fretting fatigue.* Wear and oxidation effects are slight. Accelerated crack growth can result in reduced fatigue life.
3. *Gross slip regime => Fretting wear.* Surface damage is dominated by oxidation-assisted wear. Limited crack formation is observed.
4. *Reciprocating sliding regime => Sliding wear.* For sufficiently large displacement amplitudes, the gross slip regime approaches the reciprocating sliding regime, in which wear behaviour and wear rate are similar to that of unidirectional sliding.

Vingsbo and Söderberg constructed a diagram representing a wear parameter versus the amplitude of displacements from the results of various fretting experiments (Vingsbo and Söderberg 1988). The wear parameter, called here the wear *susceptibility*, K, can be defined as the inverse of the derivative of the wear work (energy dissipation) with respect to the wear volume at a given temperature T, viz

$$K^{-1} = \left(\frac{\partial U}{\partial V}\right)_{\mathrm{T}}, \tag{1}$$

where U is the wear work and V is the wear volume. Note that U can be related to the displacement amplitude D, the normal force F and the number of cycles N, viz, $U = 2FDN$. Figure 1 displays the fretting map according to Vingsbo and Söderberg (Vingsbo and Söderberg 1988) together with the experimental data they refer to as the basis of their map but not displayed in their diagram. As can be seen from Fig. 1, even in a log-log plot the scatter in data is significant. Vingsbo and Söderberg's fretting wear threshold lines, shown in Fig. 1, do not provide a satisfactory fit to their referenced data. In other words, the threshold lines seem to be quite arbitrary. In the next section, we analyse the cause of this discrepancy.

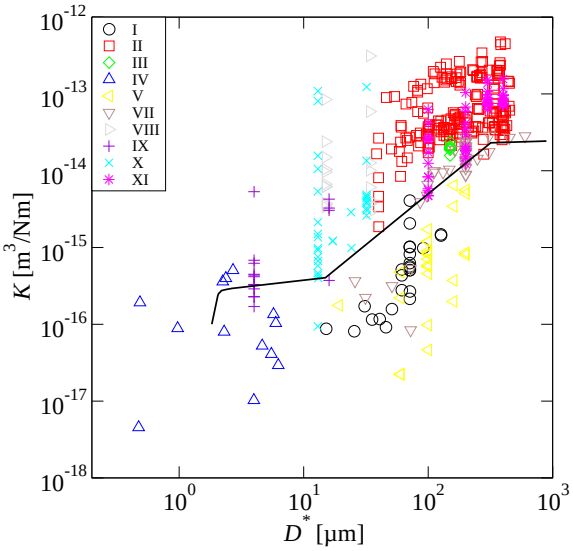

Figure 1. The wear susceptibility, K, versus the recorded displacement amplitude, D. (a) The solid line marks the fretting map according to Vingsbo and Söderberg (1988) and the symbols denote measured data; I Bill (1978), II Kayaba and Iwabuchi (1979b), III Kayaba and Iwabuchi (1981-82), IV Kennedy et al. (1984), V Kim and Lee (2003), VI Lee et al. (2001), VII Ohmae and Tsukizoe (1974), VIII Söderberg, Colvin, Salama and Vingsbo (1986), IX Söderberg, Bryggman and McCullough (1986), X Söderberg, Nikoonezhad, Salama and Vingsbo (1986) and XI Vaessen and de Gee (1968–1969).*

3 DATA ANALYSIS MODEL

A number of considerations should be made when comparing fretting wear results produced by different research groups using different test rigs and it is far beyond the scope of this paper to address all the details of the differences. The database we have considered contains four different test geometries; (*i*) sphere on flat, (*ii*) crossed cylinder, (*iii*) pin on disc and (*iv*) ring on disc (or cylinder on flat). Furthermore, fretting involves slip amplitudes on a micrometer scale, which means that the configuration of the test rig itself, or more specifically, the elastic compliance of the test rig need to be taken into account and estimated. Finally, wear is an evolving process, in the sense that material is removed from the contacting surfaces. Thus, the contact geometry changes as the wear process proceeds.

3.1 Stick regime

During the stick regime, the two bodies in contact act as one and consequently no energy is dissipated from the interface unless the bodies are plastically deformed. The peak contact pressure can be found using the Hertz contact theory

$$p_0 = \frac{3F}{2\pi xy}, \tag{2}$$

where F is the normal load and x and y are the semi-axes of an elliptic contact area. Note that in the majority of the tests included in the database, the contact area is circular with radius $x = y = a$. The contact radius is determined from the elastic and geometric properties of the interface,

$$a = \left(\frac{3FR_e}{2E_e}\right)^{1/3}, \tag{3}$$

with

$$\frac{1}{R_e} = \frac{1}{R_{1a}} + \frac{1}{R_{1b}} + \frac{1}{R_{2a}} + \frac{1}{R_{2b}}, \tag{4}$$

$$\frac{1}{E_e} = \frac{1-\nu_1^2}{E_1} + \frac{1-\nu_2^2}{E_2}, \tag{5}$$

where R_e and E_e are the equivalent radius and elastic modulus, respectively and ν is Poisson's ratio. Indices 1 and 2 refer to bodies 1 and 2 and the letter indices a and b are used to distinguish between the major and minor radius of curvature of the respective bodies. The peak contact stress exceeds the yield stress in some of the analysed experiments. Consequently, plastic deformation will take place at the interface. This plastic deformation is accounted for by increasing the respective radius of curvature.

3.2 Mixed stick-slip regime

In the mixed stick-slip regime the outer part of the contact area experiences slip during a fretting cycle. The work done by tangential forces during a complete cycle, represented by the area within the cycle loop, is dissipated by the reversal of slip within the annulus of contact. The problem was first analysed by Mindlin et al. (1951) who found an expression for the energy dissipated per cycle in a system consisting of two spherical bodies. For a sphere on a flat surface this energy, W_p, can be written as (Fouvry et al. 1995):

$$W_p = \frac{4\kappa\mu F}{a}\left[\frac{6\mu F}{5}\left(1-q^{5/3}\right) - T\left(1-q^{2/3}\right)\right], \tag{6}$$

where μ is the coefficient of friction, T is the tangential force amplitude, $q = 1 - \frac{T}{\mu F}$, and κ is the composite modulus expressed as

$$\kappa = \frac{3}{16}\left(\frac{2-\nu_1}{G_1} + \frac{2-\nu_2}{G_2}\right). \tag{7}$$

where G_1 and G_2 denote the shear moduli of the respective contacting bodies.

The tangential force amplitude is related to the partial slip displacement amplitude D_p through

$$T = \mu F \left[1 - \left(1 - \frac{aD_p}{\kappa \mu F}\right)^{3/2}\right], \tag{8}$$

$$\text{or} \quad D_p = \frac{\kappa \mu F}{a}\left[1 - \left(1 - \frac{T}{\mu F}\right)^{2/3}\right]. \tag{9}$$

The displacement amplitude of the rig D_r is assumed to depend linearly on T (Fouvry et al. 1995), viz

$$D_r = CT, \tag{10}$$

where C is the compliance of the rig. The recorded displacement amplitude D^* is assumed to be the sum of D_p and D_r

$$D^* = D_p + CT. \tag{11}$$

The transition to gross-slip occurs when $T = T_t = \mu F_t$, hence the transition amplitude to the gross slip regime is

$$D_p = D_t = \frac{\kappa \mu F_t}{a_t}. \tag{12}$$

The rig compliance C can then be found from Eq. (11)

$$C = \frac{D_t^*}{\mu F_t} - \frac{\kappa}{a_t}, \tag{13}$$

where D_t^* denotes the recorded displacement amplitude at the transition and a_t is the contact radius at transition.

Finally, substituting for T from Eq. (8) into Eq. (11) leads to an expression relating the recorded and the partial slip amplitudes through a cubic equation,

$$D^* = D_p + C\mu F \left[1 - \left(1 - \frac{aD_p}{\kappa \mu F}\right)^{3/2}\right]. \tag{14}$$

3.3 Gross slip regime

The mechanical energy dissipated during a gross slip cycle, W_g, can be split into two parts,

$$W_g = W_t + 4D_g T_t, \tag{15}$$

where W_t denotes the energy dissipated at the transition point, which is evaluated by letting $T = T_t = \mu F_t$, $q = 0$ in Eq. (6), and D_g is the gross slip amplitude. The gross slip amplitude can be found by subtracting the transition and rig amplitude from the recorded amplitude,

$$\begin{aligned} D_g &= D^* - D_t - D_r \\ &= D^* - \left(\frac{\kappa}{a_t} + C\right)\mu F_t, \end{aligned} \tag{16}$$

where we used Eq. (12) and $D_r = C\mu F_t$ at gross slip. Inserting Eq. (16) into Eq. (15) yields the final expression for the energy dissipated during a gross slip cycle

$$W_g = 4\mu F_t \left[D^* - \mu F_t \left(C + \frac{4\kappa}{5a_t}\right)\right]. \tag{17}$$

3.4 Wear volume correction

The preceding analysis, which rests on Mindlin's equations, predicts that the transition displacement amplitude to the gross slip regime is independent of the number of fretting cycles, see Eq. (12). However, many research groups have reported that a fretting system switches regimes as material is continuously worn from the surfaces, see e.g. (Söderberg, Colvin, Salama and Vingsbo 1986). Assuming that material properties remain constant, Eq. (12) states that increasing the contact area reduces the transition amplitude. Hence a system initially in the partial slip regime will eventually move into the gross slip regime.

The wear volume removed in a fretting experiment is generally very low and measurements of the material loss by weighing in many cases are not possible. Hence, indirect methods have been employed. For the crossed cylinders and ball on disc experiments, the wear volume is computed from measurements of wear scar dimensions. These computations are reversed to extract the dimensions of the wear scar. The specific methods to evaluate each experiment is commented in following section. Assuming that the profile of the worn contacting bodies can be approximated with a radius of curvature, the corresponding worn contact area is computed through Eq. (3). By matching the worn contact area with the dimensions of the wear scar it is possible to compute an updated contact radius which is then used in the above equations to compute the displacement amplitudes and energy dissipation.

3.5 Remarks on data analysis

The steps in our data analysis are summarised as follows:

1. Identify a transition point (V^*, D^*).
2. Compute the elastic compliance of the test rig (C).
3. Compute fretting amplitudes (D_p, D_t, D_g).

In the described analysis the following assumptions have been made:

(a) The surface profiles of the contacting bodies after plastic deformation and fretting wear can still be approximated with a radius of curvature.
(b) The material properties remain constant during the test.
(c) All the mechanical energy dissipated at the contact interface results in wear.

4 REPRESENTATION OF FRETTING DATA

When two surfaces in contact slide over each other, one or both of the surfaces will experience wear. A simple model describing this type of wear, originally proposed by Holm (1946) and later derived by Archard (1953) expresses the worn volume in adhesive wear, V, as

$$V = k\frac{FL}{3H_0}, \tag{18}$$

where F is the normal load, L the sliding distance, H_0 the hardness and k is called the wear coefficient, which is dimensionless and always less than unity. The factor 3 in the denominator of Eq. (18) emanates from the assumption that the worn fragment is a hemisphere.

For constructing fretting wear mechanism maps, fashioned after Lim and Ashby (1987), we introduce dimensionless variables

$$w = \frac{V}{LA}, \tag{19}$$

$$p = \frac{F}{AH_0}, \tag{20}$$

$$d = \frac{D}{a}, \tag{21}$$

where w is the normalised wear rate, p the normalised pressure, d the normalised sliding amplitude, A the contact area, D the sliding amplitude, determined according to Eqs. (14) and (16), and a the radius of the contact area.

The worn contact area and radius are used to normalise the variables to remove the dependence on the initial plasticization. Now, combining Eqs. (19) and (20) with Eq. (18), we express the wear coefficient k as

$$k = 3\frac{w}{p}. \tag{22}$$

So having determined the relations for w and p, we can find the corresponding relation for the wear coefficient through Eq. (22). This equation is a dimensionless form of the Holm-Archard relation.

Researchers define and report the sliding amplitude differently depending on the testing method. The various definitions and ranges of the sliding amplitude used are listed in Table 1. The relation between peak-to-peak amplitude, D_{p-p} and zero-to-peak amplitude, D_{0-p} is:

$$D_{p-p} = 2D_{0-p}. \tag{23}$$

Using Eq. (23), the wear susceptibility K, Eq. (1), is expressed as

$$K = \frac{V}{U} = \frac{V}{2FD_{p-p}N} = \frac{V}{4FD_{0-p}N}\ . \tag{24}$$

The data points shown in Fig. 1 are computed using the peak-to-peak amplitude definition. Hence, a mix-up in the definitions of the amplitude is one possible cause for the poor match between the threshold line and the measured data, however, this does not fully explain the prevailing deviation.

Different research groups have studied different fretting wear regions. A map is a useful tool to separate regions of different fretting wear mechanisms. However, to fully exploit the concept of fretting map, it is necessary to describe the map in terms of non-dimensional parameters. The various equipment used in these studies generate fretting wear by imparting oscillatory motions on two contacting specimens under load conditions. All these experiments were performed at room temperature in laboratory atmosphere. It should be mentioned that, from the original database referred to by Vingsbo and Söderberg (1988), we have not included the data by Bryggman and Söderberg (1986a) on niobium specimens, since these authors reported fretting wear in terms of wear scar area and not wear volume, which we have presented in Fig. 1. Similarly the data by Toth (1972) on steels were reported in terms of wear depth rate and not wear volume and no simple translation was possible, as in the case of Vaessen and de Gee (1968–1969), and therefore are not considered in the fretting map assessment here. Nevertheless, we have extended the original database with some recent data for nuclear reactor materials (Kim and Lee 2003, Lee et al. 2001). Material constants used in our assessment are given in a separate note (Knudsen and Massih 2004).

The fretting wear test database comprises the following studies; note that the Roman numerals will be used in the figures to identify the source of the data points.

I. Bill (1978) investigated the transition from mixed stick-slip to gross slip regime using a sphere on flat test geometry. The influence of the slip amplitude was further evaluated in the latter regime. AISI 9310 steel specimens were used in the tests. The frequency of vibration was set to 163 Hz and the compressive load was set to 1.47 N. From the displayed results, we identified a measured transition amplitude and wear volume of $D_t^* = 25.6\ \mu$m and $V_t = 2.37 \times 10^{-5}$ mm^3. We computed the wear volumes from scar dimensions using a spherical cap approximation, meaning that the corresponding scar radius is found from

$$h \approx \sqrt{\frac{V}{\pi R}}, \tag{25}$$

$$a = \sqrt{h(2R-h)}, \tag{26}$$

where h is the depth of the wear scar, R the sphere radius, a the scar radius; and in writing Eq. (25), we utilised $h << R$ and removed the cubic dependence on h that appears in the spherical cap formula.

II. Kayaba and Iwabuchi (1979b) studied the stick-slip and gross slip regimes and the transition to reciprocating sliding regime for sliding amplitudes in the size range of the contact zone. The materials used included commercial 0.45 wt% carbon steel and copper specimens. All the tests were made at a frequency of 16.6 Hz

using a crossed cylinder test geometry. Wear volumes were computed using the mean radius of the wear scar by integrating over an expression involving trigonometric functions, which cannot easily be inverted. However, it is found that following simple expression

$$a = \left(\frac{VR}{0.437} \right)^{1/4}, \tag{27}$$

approximates the scar radius with an error of less than 1% compared to numerically inverting Kayaba and Iwabuchi's expression for wear volume. In Eq. (27) R denotes the cylinder radius. Kayaba and Iwabuchi (1979b) identified the transition to gross slip at $D_t^* = 50$ μm for the carbon steel. Using this value, we then determined the corresponding worn volume to be $V_t = 6.6 \times 10^{-3}$ mm^3.

III. Kayaba and Iwabuchi (1981-82) investigated the influence of the surrounding temperature (20 to 650°C) on fretting wear. They found that the wear volume decreased when the temperature was increased. The materials involved in their experiments were commercial 0.45 wt% carbon steel (S45C) and 18 wt% Cr - 8 wt% Ni austenitic stainless steel (SUS 304). The test geometry consisted of an upper moving ring specimen pressed against the flat end of a cylinder specimen. All the experiments were conducted using like-metal contact combinations. Note that only data for room temperature are included in the database. Furthermore, since the data are given as the total wear volume of the two contacting surfaces, they are divided by two in order to represent the wear volume of one of the surfaces. No transition data point can be found at room temperature.

IV. Kennedy et al. (1984) studied the effect of material hardness on fretting wear in the mixed-stick slip regime. The effect of material and hardness was investigated using ball/flat combination of specimens that included AISI 52100 steel against AISI 1018 steel, a nickel chromium Hastelloy B against AISI 52100.

V. Kim and Lee (2003) made an experimental study of how the shape of the supporting springs (spacer grid) influenced fretting wear of nuclear fuel rods. Both rod and support springs were made of Zircaloy-4, a zirconium alloy. Two types of springs were included in the study, one with a concave flat contour and one with convex contour. The motion was in the axial direction of the tube. Insufficient information of the contact geometry is given to make any accurate computations regarding the contact compliance. Furthermore, the tube and springs have wall thicknesses of less than 0.5 mm, which conflicts with Mindlin's assumption of semi-infinite bodies. Hence, these data are not considered in the construction of the new map.

VI. Lee et al. (2001) studied the wear mechanisms involved in fretting wear of steam generator tubes in nuclear power plants. More specifically, they studied the effect of material combinations. Inconel 600MA and 690TT tubes were tested against two types of stainless steels (AISI 405 and 409). They used a cylinder on flat contact geometry. They found that the wear rate increased linearly with the applied normal force and the slip amplitude. However, for Inconel 690TT rubbed against stainless steel, wear transition occured above the normal load of 15N and the slip amplitude of 30 μm. By increasing the amplitude and the load beyond these values the mass loss remained constant.

VII. Ohmae and Tsukizoe (1974) investigated the effect of slip amplitude, in the range of 33-600 μm, on fretting wear. They used a square on flat test geometry, i.e. a square indenter rubbed against a flat surface. The materials used in the test were iron and 0.25 wt% steel. They found that, for a constant number of cycles, the wear volume was dependent on the slip amplitude. In particular, after 10^5 cycles, for slip amplitudes less than 70 μm, the worn volume was very small, while beyond this value it increased very rapidly. The frequency of vibration utilised in the test was 10 Hz. Wear volume data are reported for the indenter, the flat surface or as the sum of both. Since the rest of the database concerns the wear of one body only, the total wear volume data are divided by two before inclusion in the database. This operation is feasible based on the data presented in figure 5a of Ohmae and Tsukizoe (1974). We note that, Ohmae and Tsukizoe did not state which material combination was used in their tests; only they mention that two different materials were tested. In our evaluation, we used the material properties for pure iron for all the data points. Hence, these data contain an added degree of uncertainty. We found a transition point to gross slip at an amplitude of 72.1 μm with the corresponding worn volume of 1.125×10^{-3} mm^3.

VIII. Söderberg, Colvin, Salama and Vingsbo (1986) determined the transition from the mixed stick-slip to gross slip condition for low carbon steel (AISI 1018). They used a crossed cylinder test geometry. The specimens were manufactured from 12.7 mm (diameter) rod and tested in as-received condition. The transition occurred after 10^5–10^6 vibration cycles. The measurements were made at the ultrasonic testing frequency of 20 kHz.

IX. Söderberg, Bryggman and McCullough (1986) investigated the effect of the frequency of vibration on fretting wear in the mixed stick-slip regime. A low carbon steel (AISI 1018) and an austenitic stainless steel (AISI 304) were used in the test series. The employed range of frequency was 10 – 20000 Hz. The test geometry

was as in item VIII.

X. Söderberg, Nikoonezhad, Salama and Vingsbo (1986) studied the transition from the mixed stick-slip to gross slip condition and carried out further tests to evaluate the amplitude and load dependence in the latter regime. The transition occurs after 10^6–10^7 vibration cycles. The material was an austenitic stainless steel (AISI 304) and the testing frequency was 20 kHz. The experimental data reported by these authors, see also items VIII and IX, were obtained by using two different test rigs, a rig with a variable frequency in the range of 1 - 1000 Hz and an ultrasonic rig operating at 20 kHz. Both rigs used the crossed cylinder test geometry. They used Halling's equations to compute the worn volume from scar dimensions (Halling 1961), which can be inverted by solving a cubic equation for the scar depth

$$h^3 - 8Rh^2 + 16R^2h - 4\sqrt{\frac{R^3V}{\pi}} = 0, \tag{28}$$

and then extracting the scar radius from the depth by employing Eq. (26). In Eq. (28), R is the cylinder radius. Determining the elastic compliance of the ultrasonic rig for the three transition points schematically identified in (Söderberg, Nikoonezhad, Salama and Vingsbo 1986), by using Eq. (13), we find three significantly different values. Therefore, it is not possible to draw any definite conclusions regarding the compliance of the ultrasonic rig using the simplified analysis presented in section 3. Each data set is treated individually.
The compliance for the variable frequency rig is estimated from experimental data using this rig (Bryggman and Söderberg 1986b). In this experiment the transition was directly found by monitoring the tangential force. In particular they measured the transition amplitude as a function of the applied normal load. These data are fitted to Eq. (13), with $a = \sqrt{\frac{F}{\pi H_0}}$, to estimate the contact radius (Bryggman and Söderberg 1986b), viz

$$D_t^* = \mu\left(\kappa\sqrt{\pi H_0 F_t} + CF_t\right). \tag{29}$$

XI. Vaessen and de Gee (1968–1969) studied the wear rate of a "Cu-Ni-Al" pin pressed against a plain carbon steel plate (SAE 1045) for frequencies in the interval $f \in [1,40]$ Hz. The reported wear rates [μm/s] are converted to wear volumes by multiplication with the test duration time, 1 h, and the cross sectional area of the pin. It should be mentioned that no detailed information on the chemical composition of "Cu-Ni-Al" alloy is given in (Vaessen and de Gee 1968–1969). The evaluation of these data will therefore contain a higher degree of uncertainty than the other data due to lack of knowledge on the material characteristics. The deficiency in the resolution of the data points in the transition range makes the computations of the rig compliance inadmissible and thus these data cannot be used to construct the updated map.

The above described experimental data are assessed using the method described in sections 3 and 4. Note that only a subset of the database is displayed in the figures, since our method of analysis requires that the tangential compliance of the experimental rig is known (pre-calculated). Figure 2 shows the normalised wear rate w versus the normalised sliding amplitude d. The data line up in a wide band from the top left to the bottom right corner of the figure. The normalised wear rate versus the normalised pressure p is displayed in Fig. 3. Here the data points arrange in a wide band stretching from low wear rate and pressure to high wear rate and pressure. Figure 4 displays the same set of data, in the form of the displacement amplitude versus pressure. Finally, Fig. 5 depicts the data for the Holm-Archard wear coefficient k as a function of d, see Eq. (22).

5 DISCUSSION

First, let us consider the diagrams depicting the normalised wear rate, Figs. 2 and 3. The data originating from different sources fall into different regions of the diagrams. The data of Bill (1978) and Kayaba and Iwabuchi (1979b) (sets I and II) occupy the same regions of d and p. Another similarity between these data sets is that they form two groups, where the first group is characterised by high d and mid ranged p, while the second group, which is clearly separated from the former one, have lower d and higher p than the first group. However, the data by Bill (1978) display significantly lower wear rates. In Fig. 2 the data by Ohmae and Tsukizoe (1974) (set VII) align along a nearly horizontal line, i.e. close to constant wear rate, almost spanning the entire range of observed d. In Fig. 3, these data have constant p. The data from Söderberg, Colvin, Salama and Vingsbo (1986) and Söderberg, Bryggman and McCullough (1986) (sets VIII and IX) also align along lines, however with different trends, i.e.

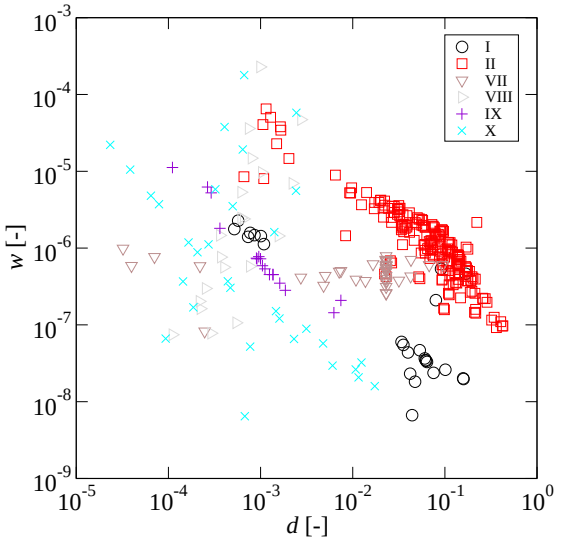

Figure 2. Normalised wear rate w versus normalised sliding displacement amplitude d. The Roman numerals in the legend are explained in the text.

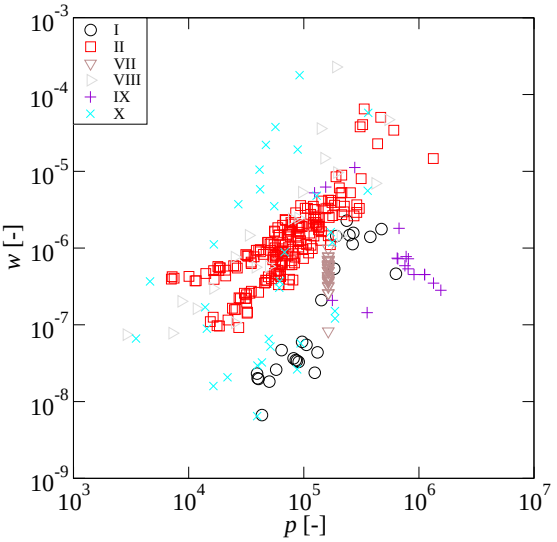

Figure 3. Normalised wear rate w versus normalised load p, cf. Fig. 2.

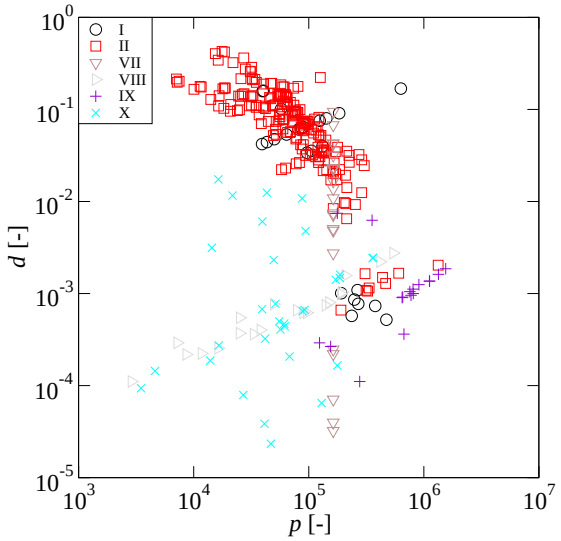

Figure 4. Normalised sliding displacement amplitude d versus normalised load p, cf. Fig. 2.

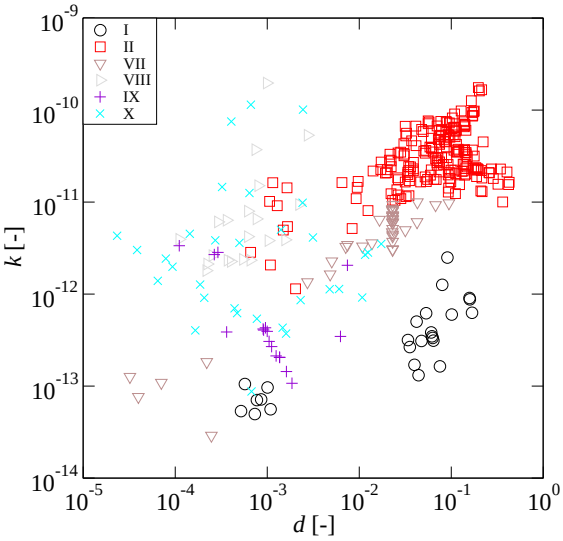

Figure 5. The wear coefficient (in the Holm-Archard formula) k versus normalised sliding displacement amplitude d, cf. Fig. 2.

data set VIII displays increasing w for increasing d and p, whereas for set IX the situation is vice versa. The last set of data, X, is sparsely distributed over the entire range of w in the lower ranges of d and p (Söderberg, Nikoonezhad, Salama and Vingsbo 1986). It should be noted that the general trend in Fig. 3, increasing w for increasing p, comply with the Holm-Archard relation, cf. Eq. (22).

Next we consider the diagram depicting normalised amplitude, d, versus normalised load, p, Fig. 4. The same data patterns as described above emerge. This figure clearly illustrates that data groups I and II occupy the same regions of (p,d) parameter space.

The data on the wear coefficient k versus d are displayed in Fig. 5. Contrary to Fig. 2 the general trend is that increasing k gives larger d. This is expected, since according to Eq. (22), k is proportional to w but inversely

Table 1. Sliding amplitudes reported by various workers.

Definition	Range [μm]	Citation
Zero-to-peak	7 – 62	Bill (1978)
Peak-to-peak	40 – 450	Kayaba and Iwabuchi (1979b)
Peak-to-peak*	150	Kayaba and Iwabuchi (1981-82)
Zero-to-peak	0 – 5	Kennedy et al. (1984)
Peak-to-peak	10 – 100	Kim and Lee (2003)
Peak-to-peak	15 – 40	Lee et al. (2001)
Peak-to-peak	33 – 600	Ohmae and Tsukizoe (1974)
Peak-to-peak	15 – 34	Söderberg, Colvin, Salama and Vingsbo (1986)
Peak-to-peak	4 – 16	Söderberg, Bryggman and McCullough (1986)
Peak-to-peak	13 – 32	Söderberg, Nikoonezhad, Salama and Vingsbo (1986)
Peak-to-peak	50 – 400	Vaessen and de Gee (1968–1969)

* Assumption according to Kayaba and Iwabuchi (1979a).

proportional to p and hence the high displacement amplitude leads to high wear and large scar area, which in turn results in lower magnitudes of p. It is worth mentioning that the values of k reported by various investigators for the adhesive wear (Rabinowicz 1995), for materials similar to the ones in our fretting database, are much larger than the values for the fretting wear depicted in Fig. 5. For example, for low carbon steel on low carbon steel, $k = 0.007$, see (Rabinowicz 1995, Hirst 1957).

The method of analysis we have utilised, enables us to separate data in the mixed stick-slip and gross slip regimes. Re-plotting Fig. 4 by separating these regimes leads to the results shown in Fig. 6. Next, inserting the relations for the normalised amplitude, Eq. (21), and the load, Eq. (20), into Eq. (12) yields

$$d_t = \frac{\kappa\mu}{a_t^2} A H_0 p_t. \tag{30}$$

Moreover, assuming that we have a like metal pair and a circular contact area, Eq. (30) is re-expressed as

$$d_t = \frac{3\pi\mu(2-\nu)H_0}{8G} p_t, \tag{31}$$

where Eq. (7) was utilised. Equation (31) relates the transition amplitude to the transition load via the elastic constants, ν, H_0 and G. As an example, the material properties for the AISI 9310 steel are used to draw the transition line shown in Fig. 6, i.e. $d_t \approx 5.257 \times 10^{-9} p_t$.

Next, let us return to the diagrams involving the normalised wear rate w, Figs. 2 and 3. Once again the data points are separated into the gross and mixed stick-slip regimes, see Figs. 7 and 8. Comparing these results and considering that $d_t \sim p_t$, it is clear that a power law expression cannot be used to relate the transition wear rate w_t versus d_t or p_t. Instead a pragmatic approach is adopted, that is we observe that the mixed stick-slip data fall in the top left corner of Fig. 7. The location of the boundary lines is found by ensuring that the number of gross slip points that fall into the mixed stick-slip region equals the number of mixed stick-slip points that fall into the gross slip region. The resulting transition boundary is included in Fig. 7. Finally, using the same approach as w versus d, a transition boundary is also drawn in Fig. 8 for the w versus p data.

6 CONCLUDING REMARKS

From the discussions in the preceding sections, it is clear that fretting wear is an evolving process in the sense that the fretting mechanism can change as the wear process proceeds. This makes it hard to implement the concept

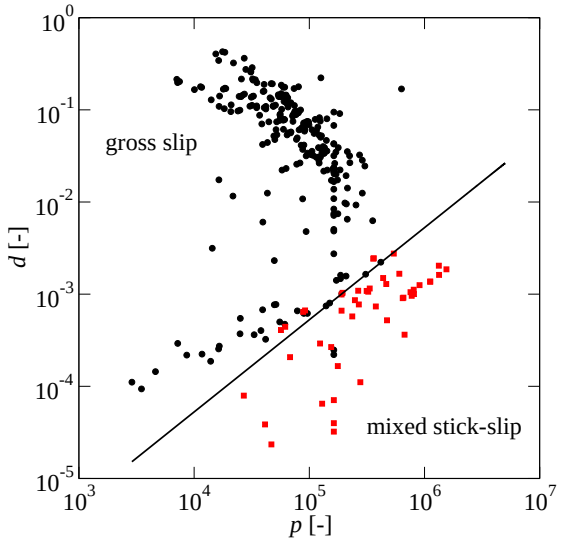

Figure 6. Normalised sliding displacement amplitude d versus normalised load p. Black circles and red squares denote gross slip and mixed stick-slip data, respectively. The transition line is drawn for AISI 9310 material properties.

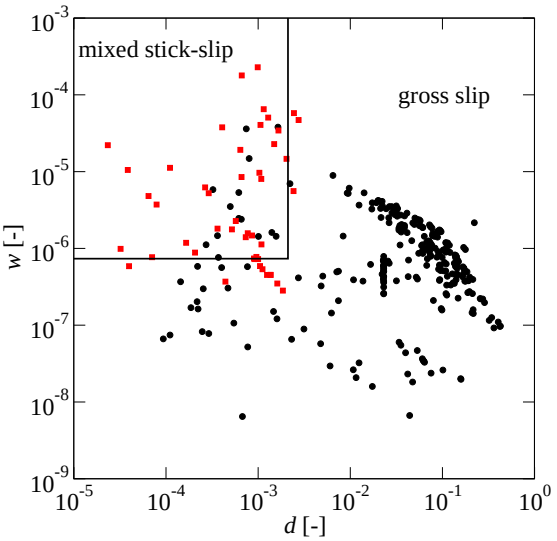

Figure 7. Normalised wear rate w versus normalised sliding displacement amplitude d. Black circles and red squares denote gross slip and mixed stick-slip data, respectively. The solid line marks the estimated transition between mixed stick-slip and gross slip regimes.

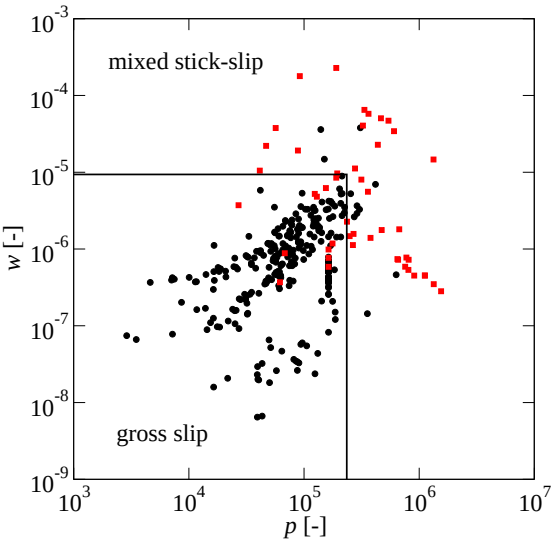

Figure 8. Normalised wear rate w versus normalised load p. Black circles and red squares denote gross slip and mixed stick-slip data, respectively. The solid line marks the estimated transition between mixed stick-slip and gross slip regimes.

of fretting map, at least with the intention to distinguish fretting wear regimes, using the original configuration as reference. The problem can be treated by introducing a transition domain, the mixed slip domain, to identify the conditions where the system switches from mixed stick-slip to gross slip or vice versa, e.g. (Fouvry, Kapsa and Vincent 1998). In our study, this is tackled by using the scar size as an estimate of the contact area. The proposed analysis method enables a comparison between various experimental data provided that the tangential compliance of the experimental rig can be estimated. The map parameters should be expressed in non-dimensional form. There

are two possible routes to chose these parameters; (*a*) an empirical approach and (*b*) a model based approach. Both approaches were attempted here. The following points need to be considered when selecting the map parameters:

Parameter space. The fretting wear parameters need to be "independent" of each other. Lim and Ashby (1987) used normalised (non-dimensional) force and velocity to construct a wear-mechanism map based on steady-state sliding wear pin-on-disk experiments. For the pin-on-disk experiment the nominal contact area is just the cross-section area of the pin which is a geometric constant of the test set-up. Here, we have used the contact area, to normalise load and velocity. Hence, for incomplete contacts (e.g. crossed cylinder, sphere on flat surface), both parameters become load dependent. The fretting parameter space considered here is 3-dimensional, expressed as $\mathbf{q} = (w, d, p)$.

Heat generation. Heat is generated at the sliding interface during fretting. This local heating is substantial, especially in high-frequency experiments. For example, interface temperatures above 800°C have been reported in the literature for an experiment conducted at room temperature (Söderberg, Colvin, Salama and Vingsbo 1986).

Physical relevance. It is important that the chosen parameters have physical relevance, i.e. they should be based on measurable quantities describing the phenomenon.

Map dimension. The dimension of the map needs to be considered. The present paper describes an attempt to construct a two dimensional map. A third axis, is however, necessary to fully capture the evolutionary nature of fretting systems. This is the purpose of the RCFM (Vincent et al. 1992).

The above considerations suggest that both mechanistic modelling and more accurate fretting data are needed to delineate distinctly the different regimes of fretting wear. Also, constructing three dimensional maps can aid to understand the role of important fretting wear parameters. Recent advances in modelling arbitrary shaped contact surfaces using either numerical methods, e.g. (Johansson 1994) or semi-analytical procedures (McVeigh, Harish, Farris and Szolwinski 1999, Kim and Lee 2003), can be employed to compare different fretting experiments more accurately. Furthermore, these methods may be used, together with an appropriate wear model, to predict the transition point (d_t, p_t) in the mixed slip regime by evaluating the changing contact geometry due to wear.

Acknowledgements The work was supported by the Swedish Foundation for Knowledge and Competence Development (KKS) under Award HÖG 212/01.

REFERENCES

Archard, J.: 1953, Contact and rubbing of flat surfaces, *Journal of Applied Physics* **24**, 981–988.

Au-Yang, M. K.: 2001, *Flow-Induced Vibration of Power and Process Plant Components*, Professional Engineering Publishing Limited, Suffolk, UK.

Bill, R. C.: 1978, Fretting AISI 9310 steel and selected fretting-resistant surface treatments, *ASLE Transactions* **21**, 236–242.

Bryggman, U. and Söderberg, S.: 1986a, Contact conditions and surface degradation mechanisms in low-amplitude fretting, *Technical Report UPTEC 86 66R*, School of Engineering, Uppsala University, Uppsala, Sweden.

Bryggman, U. and Söderberg, S.: 1986b, Contact conditions in fretting, *Wear* **110**, 1–17.

Dahmani, N., Vincent, L., Vannes, B., Berthier, Y. and Godet, M.: 1992, Velocity accomodation in polymer fretting, *Wear* **158**, 15–28.

Fisher, N. J., Chow, A. B. and Weckwerth, M. K.: 1994, Experimental fretting-wear studies of steam generator materials, *Flow-Induced Vibration*, Vol. 273 of *PVP*, ASME, pp. 241–255.

Fisher, N. J., Chow, A. B. and Weckwerth, M. K.: 1995, Experimental fretting-wear studies of steam generator materials, *Journal of Pressure Vessel Technology* **117**, 312–320.

Fouvry, S., Kapsa, P. and Vincent, L.: 1995, Analysis of sliding behavoiur for fretting loadings: determination of transition criteria, *Wear* **185**, 35–46.

Fouvry, S., Kapsa, P. and Vincent, L.: 1996, Quantification of fretting damage, *Wear* **200**, 186–205.

Fouvry, S., Kapsa, P. and Vincent, L.: 1998, Developments of fretting sliding criteria to quantify the local friction coefficient evolution under partial slip condition, *in* D. Dowson (ed.), *Tribology for energy conservation*, Elsevier Science B.V.

Fouvry, S., Kapsa, P., Vincent, L. and Dang Van, L.: 1996, Theoretical analysis of fatigue cracking under dry friction for fretting loading conditions, *Wear* **195**, 21–34.

Halling, J.: 1961, A crossed-cylinder wear machine and its use in the study of severe wear of brass on mild steel, *Wear* **4**, 22–31.

Hirst, W.: 1957, Wear of unlubricated metals, *Proceedings of the Conference on Lubrication and Wear*, The Institution of Mechanical Engineers, London, pp. 674–681.
Holm, R.: 1946, *Electric contacts*, Almqvist and Wiksells, Stockholm, Sweden.
Hutchings, I. M.: 1992, *Tribology*, Edward Arnold, London, UK.
Johansson, L.: 1994, Numerical simulation of contact pressure evolution in fretting, *Journal of Tribology* **116**, 247–254. Transactions of the ASME.
Johnson, K. L.: 1995, Contact mechanics and the wear of metals, *Wear* **190**, 162–170.
Kayaba, T. and Iwabuchi, A.: 1979a, Influence of hardness on fretting wear, *in* K. C. Ludema (ed.), *Proceedings of international conference on wear of materials 1979, Dearborn, Michigan*, ASME, New-York, pp. 371–378.
Kayaba, T. and Iwabuchi, A.: 1979b, On the effects of slip amplitude on fretting wear, *Technology Reports, Tohuku University* **44**(2), 603–623.
Kayaba, T. and Iwabuchi, A.: 1981-82, The fretting wear of 0.45%C steel and austenitic stainless steel from 20 to 650°C in air, *Wear* **74**(2), 229–245.
Kennedy, P. J., Stallings, I. and Peterson, M. B.: 1984, A study of surface damage at low-amplitude slip, *ASLE Transactions* **27**, 305–312.
Kim, H.-K. and Lee, Y.-H.: 2003, Influence of contact shape and supporting condition on tube fretting wear, *Wear* **255**, 1183–1197.
Knudsen, J. and Massih, A. R.: 2004, Material properties for fretting wear database, *Technical Report MUMAT 2004:1*, Materials Science, Malmö Högskola, Malmö, Sweden. Available from authors.
Lee, Y.-H., Kim, I.-S., Kang, S.-S. and Chung, H.-D.: 2001, A study on wear coefficients and mechanisms of steam generator tube materials, *Wear* **250**, 718–725.
Lim, S. C. and Ashby, M. F.: 1987, Wear-mechanisms maps, *Acta Metallurgica* **35**, 1–24.
McVeigh, P. A., Harish, G., Farris, T. N. and Szolwinski, M. P.: 1999, Modeling interfacial conditions in nominally flat contacts for application to fretting fatigue of turbine engine components, *International Journal of Fatigue* **21**, S157–S165.
Mindlin, R. D.: 1949, Compliance of elastic bodies in contact, *Journal of Applied Mechanics* pp. 259–268.
Mindlin, R. D. and Deresiewicz, H.: 1953, Elastic spheres in contact under varying oblique forces, *Journal of Applied Mechanics* pp. 327–344.
Mindlin, R. D., Mason, W. P., Osmer, T. F. and Deresiewicz, H.: 1951, Effects of an oscillating tangential force on the contact surfaces of elastic spheres, *Proceedings: First US National Congress of Applied Mechanics*, pp. 203–208.
Odfalk, M. and Vingsbo, O.: 1990, Influence of normal force and frequency in fretting, *Tribology transactions* **33**(4), 604–610.
Ohmae, N. and Tsukizoe, T.: 1974, The effect of slip amplitude on fretting, *Wear* **27**, 281–294.
Pettigrew, M. J., Taylor, C. E., Fisher, N. J., Yetsir, M. and Smith, B. A. W.: 1998, Flow-induced vibration: recent findings and open questions, *Nuclear Engineering and Design* **185**, 249–276.
Rabinowicz, E.: 1995, *Friction and Wear of Materials*, 2nd edn, John Wiley & Sons, New York. Chap. 6.
Söderberg, S., Bryggman, U. and McCullough, T.: 1986, Frequency effects in fretting wear, *Wear* **110**, 19–34.
Söderberg, S., Colvin, T., Salama, K. and Vingsbo, O.: 1986, Ultrasonic fretting wear of plain carbon steel, *Journal of Engineering Materials and Technology* **108**, 153–158.
Söderberg, S., Nikoonezhad, S., Salama, K. and Vingsbo, O.: 1986, Accelerated fretting wear testing using ultrasonics, *Ultrasonics* **24**, 348–353.
Szolwinski, M. P. and Farris, T. N.: 1996, Mechanics of fretting fatigue crack formation, *Wear* **198**, 93–107.
Toth, L.: 1972, The investigation of the steady stage of steel fretting, *Wear* **20**, 277–286.
Turki, C., Salvia, M. and Vincent, L.: 1993, Fretting maps of glass fiber - reinforced composites, *in* T. Chandra and A. K. Dhingra (eds), *Proceedings Advanced Composites 93, International Conference on Advanced Composite Materials, 1993*, The Minerals, Metals& Society, Wollongong, pp. 1419–1424.
Vaessen, G. H. G.and Commissaris, C. P. L. and de Gee, A. W. J.: 1968–1969, Fretting corrosion of Cu-Ni-Al against plain carbon steel, *Proceedings of the Institution of Mechanical Engineers* **183**, 125–128.
Vincent, L., Berthier, Y. and Godet, M.: 1992, Testing methods in fretting fatigue: A critical appraisal, *in* M. H. Attia and R. B. Waterhouse (eds), *Standardization of Fretting Fatigue Test Methods and Equipment, ASTM STP 1159*, American Society for Testing and Materials, Philadelphia, pp. 33–48.
Vingsbo, O., Odfalk, M. and Shen, N.-E.: 1990, Fretting maps and fretting behaviour of some f.c.c. metal alloys, *Wear* **138**, 152–167.
Vingsbo, O. and Söderberg, S.: 1988, On fretting maps, *Wear* **126**, 131–147.

